Vol. 68: 151–167, 2016
doi: 10.3354/cr01393

CLIMATE RESEARCH
Clim Res

Published May 4

Contribution to CR Special 32 'CLARIS-La Plata Basin: climate variability and uncertainties'

Changes in temperature extremes for 21st century scenarios over South America derived from a multi-model ensemble of regional climate models

Noelia López-Franca[1,2,*], Pablo G. Zaninelli[1,2], Andrea F. Carril[1,2], Claudio G. Menéndez[1,2,3], Enrique Sánchez[4]

[1]Centro de Investigaciones del Mar y la Atmósfera (CIMA/CONICET-UBA), Buenos Aires, Argentina
[2]Instituto Franco-Argentino para el Estudio del Clima y sus Impactos (UMI IFAECI/CNRS-CONICET-UBA), Buenos Aires, Argentina
[3]Departamento de Ciencias de la Atmósfera y los Océanos (DCAO/FCEN/UBA), Buenos Aires, Argentina
[4]Universidad de Castilla-La Mancha, Av. Carlos III s/n., 45071 Toledo, Spain

ABSTRACT: This study examines a set of 4 temperature extreme indices (cold and warm nighttime and daytime indices) from an ensemble of 4 regional climate models (RCMs) for present and future periods in South America (SA). These models were integrated in the framework of the CLARIS-LPB 7FP-EU-project. We analyze the capability of RCMs to reproduce such indices and explore changes projected by the models under the scenario A1B for the end of the 21st century. The work also analyzes the role of cloudiness, surface radiative forcing and meridional wind components on temperature extremes. Future projections show that, during the austral summer, the increase in the frequency of warm nights is larger than that projected for warm days. This result agrees with the projections for the seasonal mean fields of minimum temperature (TN) versus the maximum temperature (TX) over most of SA. The analysis for the La Plata Basin suggests that this behavior is consistent with the cooling effect of cloud cover affecting TX, while TN is affected by nighttime greenhouse warming. The relationship between cloudiness and TN and TX anomalies shows a nonlinear behavior for near full cloud cover conditions. Although TX and TN anomalies are sensitive to strong cold air advection, TX is more sensitive than TN. Thus, RCMs are useful tools to analyze both the spatial pattern of temperature extremes and the climatic factors involved.

KEY WORDS: Temperature extremes · South America · Climate change · Regional climate models · Multi-model ensemble

1. INTRODUCTION

The study of extreme climate impacts over the 21st century has become a key focus of climate research due to their long-lasting social and environmental consequences. Extreme impacts are commonly caused by extreme climatic events, although non-climatic events (e.g. wildfire) or even the persistence of a certain conditions (e.g. dry days) also can lead to an extreme impact. A comprehensive study of extreme climatic events is necessary to assess their positive or negative effects on physical, ecological and human systems (Lavell et al. 2012). There are different ways to define an extreme event, based on its rarity, intensity and the damage caused (Beniston & Stephenson 2004). In particular, the intensity of these events as identified from distribution tails is considered more relevant to society and natural systems than aspects related to the frequency (Zhang et al. 2011).

*Corresponding author: noelia.lopezfranca@cima.fcen.uba.ar

Temperature extremes are often described through indices related to their intensity, in terms of their maxima or magnitudes above or below defined thresholds (Stephenson 2008). Frich et al. (2002) describe a suite of extreme magnitudes defined by the Expert Team on Climate Change Detection and Indices (ETCCDI, http://etccdi.pacificclimate.org) in order to quantify changes in climate extremes with respect to a baseline period. Among them, minimum and maximum temperature indices and the tails of temperature distributions (10th and 90th percentiles) have been widely used to analyze changes in the occurrence of warm/cold days/nights over different regions of the world (Alexander et al. 2006, Aguilar et al. 2009, You et al. 2011, Andrade et al. 2012, Skansi et al. 2013). Such changes could have direct impacts on human health through thermal stress caused by the occurrence of persistent warm temperatures (during the day and night time) over several days. Increased temperatures may also increase energy and water demand (Bambrick et al. 2011), and particularly affect economic sectors that carry out their activities outdoors (agriculture, tourism, the building sector, among others).

The fifth IPCC report (Hartmann et al. 2013) underlines warming changes in daily temperature, larger in minimum (TN) than in maximum temperatures (TX) over the whole globe since the mid-20th century. While the frequency of occurrence of warm days/nights has shown an increase, that of the cold days/nights presents a decrease for that period. These changes in the frequency of temperature extremes are likely to be related to the asymmetric behavior of TN and TX percentiles (Beniston & Stephenson 2004). South America (SA) is one of the world regions for which the strongest reductions in cold-night frequency have occurred during the 20th century (Vincent et al. 2005, Alexander et al. 2006, Donat et al. 2013), with a hotspot in the Amazon basin (Rusticucci 2012, Skansi et al. 2013). Under climate change conditions, similar changes are projected by CMIP3 (Marengo et al. 2009) and CMIP5 global climate models (GCMs) (Sillmann et al. 2013b). Specifically, (1) changes are expected to be larger in TN than in TX extremes and (2) and increases in the highest percentiles of TX and TN are projected to be larger than those in the respective lowest percentiles (Kodra & Ganguly 2014). Moreover, the largest changes are projected in tropical regions and the smallest ones in southern SA (Sillmann et al. 2013b).

In order to understand the causes of these extremes events, it is necessary to identify the climatic factors involved, and how they could evolve under climate change conditions. Changes in the occurrence of warm/cold days/nights show large correlations with TN and TX changes (Rusticucci & Barrucand 2004), resulting in a decreasing trend in the diurnal temperature range (DTR), with the magnitude of the change being comparable to the mean warming itself (Stone & Weaver 2003). DTR is largely influenced by cloudiness, water vapor and soil moisture (Dai et al. 1999, Andrade et al. 2012). These factors together with surface winds and energy fluxes are relevant in the analysis of daily temperature extremes. During daytime, clouds exert an albedo effect on the temperature, (i.e. TX), thereby reducing net surface downward shortwave radiation (SWR) from the sun. At night, clouds play a greenhouse role, enhancing the net surface downward longwave radiation (LWR) and hence increasing the temperature (i.e. TN). Thus the combined effect of these factors can cause a decrease in the DTR (Rangwala et al. 2012). Variations in surface wind direction may also affect DTR through advection of air masses with different temperatures and humidity (Garreaud 2000, Dai et al. 1999, Plavcová & Kyselý 2011). These factors can vary annual and seasonally (Andrade et al. 2012, Betts et al. 2013).

Under climate change conditions, the GCMs project decreases of DTR over most of the land regions of the world (Lindvall & Svensson 2014). This change corresponds well in terms of spatial pattern and magnitude with increases in the cloudiness and decreases of SWR, but a weaker correlation exists between DTR and LWR, as it projects larger increases (Zhou et al. 2009). These studies identify the La Plata Basin (LPB) as the region of SA where the largest decreases in DTR are projected in the future. Among the main factors cited above, Zaninelli et al. (2015) found large correlations between components of the energy flux balance and daily temperatures (TN and TX), using there the observational gridded dataset developed by Tencer et al. (2011) for southeastern SA, including the LPB.

Regional climate models (RCMs) allow appraisal of the possible future changes of daily temperature extremes and their contributory factors at local and regional scales (Zhou et al. 2009, Andrade et al. 2012, Plavcová & Kyselý 2012). As SA is considered as a climate-data-sparse region (Menéndez et al. 2010a, Tencer et al. 2011, Rusticucci 2012, Skansi et al. 2013), RCMs could represent a useful tool for the climatological study of extreme events. The ensemble of RCMs over this region has been shown to be a very interesting tool for these studies (Menéndez et al. 2010b). Results from the CLARIS-LPB European–

South American project have already been assessed under present reanalysis-forced conditions (Solman et al. 2013) and for GCM-forced conditions (Sánchez et al. 2015), with successful results in terms of their description of the overall and subregional spatial and annual patterns of seasonal mean temperature and precipitation.

This work focuses on the analyses of ETCCDI indices of daily minimum and maximum temperatures and warm/cold day/nights over the whole SA, based on an observational database, multi-decadal reanalyses and a multi-model ensemble of regional climate model simulations. All these results are used to quantify the uncertainty in reproducing extreme indices. Moreover, the factors involved in the occurrence of extremes over the LPB region are analyzed. Among the possible climatic factors, the study focuses on the role of cloudiness, surface radiative forcing and meridional wind component. The analysis is made for the austral summer (DJF) and winter (JJA) seasons, and performed considering near present and future climate conditions.

2. DATA AND METHODS

Analyses are performed using a multi-model ensemble (RCM-ENS) composed of 4 RCMs driven by 3 coupled GCMs: LMDZ (Li 1999) driven by IPSL (Hourdin et al. 2006), PROMES (Castro et al. 1993) driven by HadCM3 (Gordon et al. 2000) and RCA (Samuelsson et al. 2011) and REMO (Jacob et al. 2012) driven by EC5OM (Roeckner et al. 2006). A description of the models can be found in Solman et al. (2013). Models were focused over the SA domain with horizontal resolution of about 50 km, covering the 1961–2099 time period. The models selected for this study are those which have daily data of the studied variables (TN, TX, LW, SW and meridional wind at 850 hPa). The analysis is performed considering 2 periods: near present (1991–2010) and future climate conditions (2079–2098). The near-present period was composed of a 10 yr run (1991–2000) forced by historical changes in the atmospheric composition, reflecting both anthropogenic and natural sources (i.e. a 20th century reanalysis [20CR] experiment), concatenated with another 10 yr run (2001–2010) forced by SRES A1B atmospheric concentrations (Nakicenovic et al. 2000). The reason for this approach is because the near present period did not overlap with the base period (1961–1990) defined for estimation of the threshold values of extremes indices (Zhang et al. 2011). Future climate conditions are simulated under the SRES A1B greenhouse gas scenario. The climate change signal is computed then as the difference between the future (2079–2098) and near present (1991–2010) periods.

The Climatic Research Unit (CRU) version TS3.21 (Harris et al. 2014) gridded monthly observational database, with a spatial resolution of 0.5°, is used to check the ability of the climate models to reproduce the spatial patterns of temperature. Fig. 1 (top panels) shows the biases in the base period 1961–1990 in seasonal mean surface air temperature of RCM-ENS and the ensemble of GCM forcing models (bottom panels) for DJF and JJA and projected changes in mean temperature (2079–2098 minus 1991–2010) according to regional and global models. Comparing the biases provides a rough idea of the added value of RCMs compared to GCMs. Biases tend to be lower for RCMs (Fig. 1b,d) than for GCMs (Fig. 1a,c) for both seasons, with a few exceptions, such as in southern LPB (region marked with a rectangle in the Fig. 1), where they are similar. The geographical distribution of biases is qualitatively similar for the RCM and GCM ensembles, excluding the LPB in JJA (Fig. 1c,d), but with a cold bias for the coupled models and a warm bias for RCM-ENS. In general, temperature biases have opposite signs in the LPB and eastern Brazil. Errors are relatively large in the southern LPB for both ensembles, particularly during DJF (Fig. 1a,b). In most cases, RCM and GCM simulations are too dry (not shown) and too warm in their present climate simulations during summer in the LPB. Among the factors that could exacerbate this problem, the southern LPB is an area of strong coupling between the land surface and the atmosphere (Sörensson & Menéndez 2011), and therefore errors in the simulation of precipitation directly affect the temperature through feedbacks with soil moisture and evapotranspiration (Menéndez et al. 2016, this Special). In winter, and land surface–atmosphere coupling is less important (Ruscica et al. 2016); the reasons behind these errors still need to be investigated. When interpreting results of models, it is useful to examine how the climate change signal is modified by the RCM-ENS. Projected seasonal mean temperature changes simulated by global models (Fig. 1e,g) are modified by dynamic downscaling with the regional models (Fig. 1f,h). In both seasons, differences in the geographical distribution of warming between both ensembles are observed. The RCM-ENS exhibits greater warming compared to global models, particularly in Bolivia, the northern LPB and southern Brazil. By contrast, in Amazonia in DJF and Eastern Brazil in JJA, RCM-ENS simulates less warming

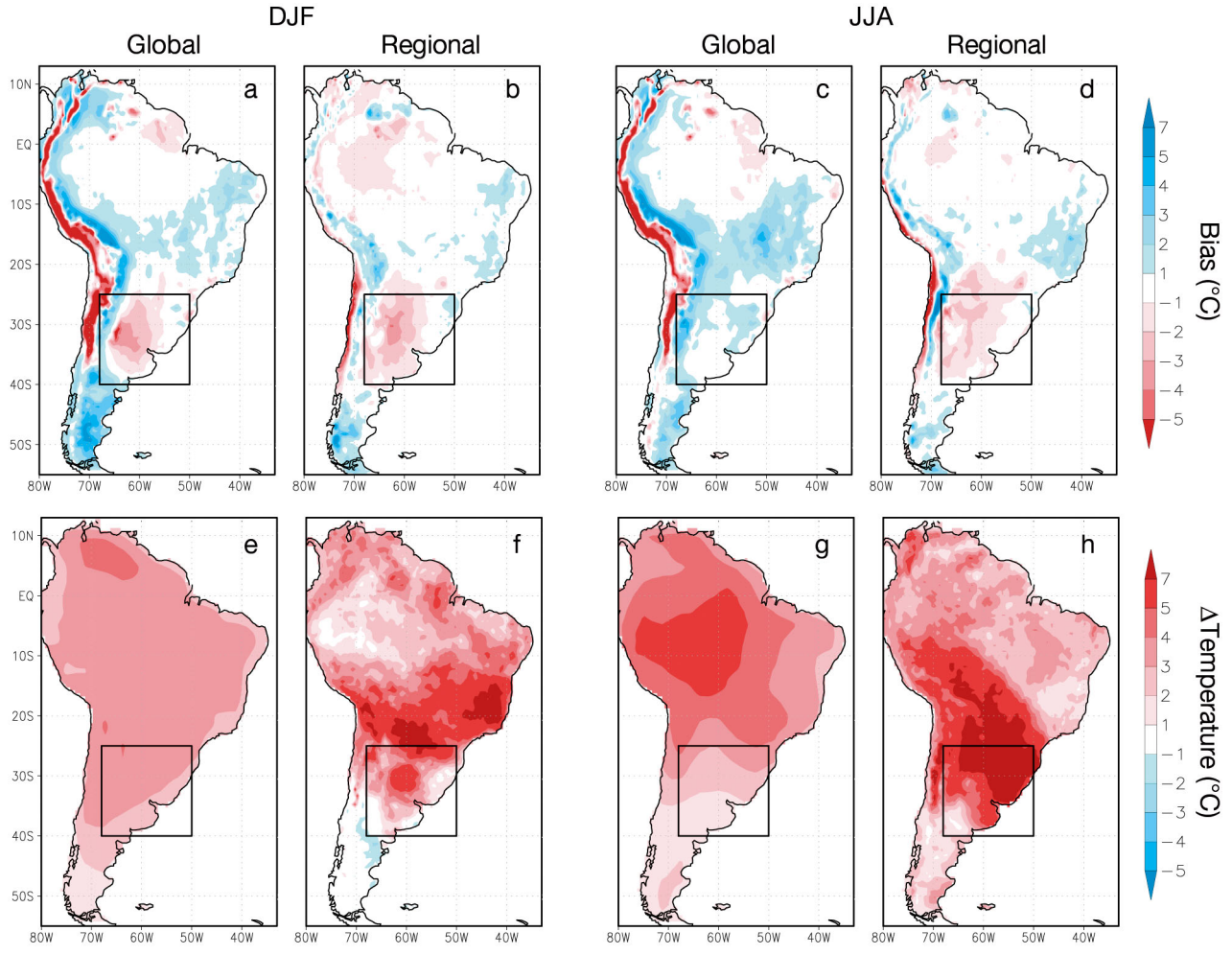

Fig. 1. Seasonal mean surface air temperature bias (°C) of ensembles of global and regional models. Top panels: Difference between the Climatic Research Unit (CRU) gridded monthly observational database (Harris et al. 2014) and simulated austral summer (DJF) and winter (JJA) values for the 1961–1900 period. (a) Global ensemble, DJF; (b) regional ensemble (RCM-ENS), DJF; (c) global ensemble, JJA; (d) RCM-ENS, JJA. Bottom panels: Changes projected by global and regional models (2079–2098 minus 1991–2010, SRES A1B). (e) Global ensemble, DJF; (f) RCM-ENS, DJF; (g) global ensemble, JJA; (h) RCM-ENS, JJA. The box indicates the La Plata Basin (LPB) subdomain selected for detailed analysis

than GCMs. The higher spatial resolutions of RCMs result in higher spatial variability in climate responses compared with those from GCMs. Sánchez et al. (2015) analyze the biases and climatic signals of individual models used in the CLARIS LPB project. The inter-model spread is relatively large, especially for regional models, suggesting that the results of RCM-ENS could be sensitive to the choice of individual models that compose it.

A statistical summary of how well the models simulate the seasonal geographical patterns of TX and TN in terms of the centered root mean square difference (RMSD), the correlation coefficient (R) and the standard deviation (SD) is described by means of Taylor diagrams (Taylor 2001). These diagrams (see Fig. 2) provide a visual framework to easily compare results between models and gridded observations. Points in the diagram represent the statistical values for a model and for the climatology of reference. The radial distance from the origin is proportional to STD, the radial distance from the reference climatology (CRU, black point in Fig. 2) is proportional to the centered RMSD and the correlation between each single model/ensemble and the reference climatology is given by the azimuthal position. Taylor diagrams are calculated over the full SA domain for DJF and JJA, and the statistics are obtained after removing the spatial mean value of each database or model.

To date, there is no direct daily gridded observational dataset of surface temperature covering the whole SA domain available. Therefore, the HadEX2 gridded observational-based extremes dataset, docu-

Table 1. Expert Team on Climate Change Detection and Indices (ETCCDI) definitions of extreme temperature indices. Units are percent for all indices

ID	Name	Description
TN10p	Cold nights	Percentage of days when TN < 10th percentile
TX10p	Cold days	Percentage of days when TX < 10th percentile
TN90p	Warm nights	Percentage of days when TN > 90th percentile
TX90p	Warm days	Percentage of days when TX > 90th percentile

mented in detail in Donat et al. (2013) and available from the CLIMDEX project website (www.climdex.org/), is used to evaluate RCM-ENS extremes. This dataset is based on climate extremes indices defined by the ETCCDI (Zhang et al. 2011), in which the percentile-based threshold are derived from the 1961–1990 period. Indices selected here are those related with diurnal and nocturnal temperature extremes (see Table 1). HadEX2 is available on a 2.5° × 3.75° longitude–latitude grid and has been previously used by other authors (e.g. Flato et al. 2013, Sillmann et al. 2013a, 2014, Thibeault & Seth 2014). One of the main constraints of HadEX2 is the spatial coverage based on the station network. Moreover, as noted by Sillmann et al (2013a), indices are calculated directly from station-based observations and then interpolated to a global grid, which results in a spatial-scale mismatch with indices calculated from model output because the latter represents area (grid box) averages rather than point values. Therefore, we complement the HadEX2 indices with extremes computed from the National Center for Environmental Prediction/National Center for Atmospheric Research (NCEP/NCAR) Reanalysis 1 (NCEP1) (Kalnay et al. 1996) and the second Japanese global atmospheric reanalysis (JRA-55) (Kobayashi et al. 2015). Both reanalyses are obtained from the CISL Research Data Archive (http://rda.ucar.edu/). NCEP1 data is available on a 192 × 94 Gaussian grid and JRA-55 on a 640 × 320 Gaussian grid (no other reanalysis is available for the period 1961–2010 that provides daily data over SA). All the datasets have been interpolated to a common grid (0.5° × 0.5°) to ensure consistency among them.

Following Giorgi & Francisco (2000, their Table 2), temporal and spatial averaged statistics of extremes have been estimated over 2 sub-regions of SA: north South America (NSA, north of 20°S) and south South America (SSA, south of 20°S). For each extreme index and for each dataset, a space- and time-varying mask according to the HadEX2 data availability has been applied in order to properly compare indices from RCM-ENS and reanalysis with those of HadEX2. Results are summarized by box-and-whisker plots for each dataset (see Fig. 4). The validation of the simulated spatial patterns of the extreme indices is done against HadEX2 and reanalysis.

Use of multi-model averages to enhance signals is common practice (see e.g. Carril et al. 2012). Therefore, the climate change projection of TN, TX and extreme temperature indices are displayed as the multi-model ensemble mean difference between future and near present periods, identifying regions with statistically significant signal-to-noise ratio (SNR), i.e. the signal due to anthropogenic gases increases versus the noise from individual models. Following Kendon et al. (2008), SNR is defined as:

$$\mathrm{SNR} = \frac{\overline{F} - \overline{P}}{\sqrt{(\sigma_P^2 + \sigma_F^2)\,/\,2'}} \qquad (1)$$

where the numerator indicates the projected average change, calculated as the different between future (F) and near present conditions (P), while σ_P^2 and σ_F^2 in the denominator represent the variances across the ensemble for each time slice. To interpret SNR in terms of its significance, a Student t-test with $\alpha = 0.05$ is applied, where the null hypothesis indicates that values between near present and future are different.

There are different processes and climatic variables that could affect surface air temperature, and consequently, its extremes. In the context of climate change, these variables are changing and also interacting with each other. In particular, the characteristics of the temperature fields in the LPB are closely related to both the large-scale circulation and the synoptic conditions that transport heat in a meridional direction (Garreaud et al. 2009). Therefore, based on the RCM-ENS, the influence of cloud cover, radiation fluxes and winds on temperature and its projections are investigated for the area-averaged LPB domain (25° S to 40° S, 50° W to 68° W). Considered variables are total cloud cover (TCC), SWR, LWR, surface net radiation (Rn) and 850 hPa meridional wind component (v850). Rn is defined as the sum of SWR and LWR, and the DTR as the difference between TX and TN. We chose the wind at the 850 hPa level because this is usually above the boundary layer, but not too far from the surface, where the extremes actually occur (Andrade et al. 2012). To examine the influence of these variables on TX and TN changes, the following computations are made. In analogy with the procedure used to obtain the extreme indices, daily temperature and wind

anomalies are computed as deviations from the seasonal mean baseline period value. Therefore, daily temperature anomalies are grouped with daily meridional wind at 850 hPa. Moreover, as RCMs provide a set of physically consistent variables, the joint variability among the TCC, surface radiation budget (Rn, SWR and LWR), temperature fields (TN, TX) and DTR is quantified for both the near-present and future periods. This analysis is a contribution towards better understanding of temperature changes in the LPB region.

3. RESULTS AND DISCUSSION

3.1. Seasonal mean fields of minimum and maximum temperature

Taylor diagrams for TN and TX (Fig. 2) show that RCM-ENS (red point) has a good performance relative to each individual model (red dots are further away from the outlier points and near to the cluster of best models). As in e.g. Carril et al. (2012) and Menéndez et al. (2010a), combining models in a multimodel ensemble gives a better climate description than any individual model, independently of the variable and the season. The regional models capture better the spatial characteristics of TN than those of TX: the spread between models is large for TX, with PROMES being the outlier model in this case. Note, however, that reanalysis errors are comparable to RCM-ENS. This simple analysis provides a crude but useful measure of uncertainty to put the magnitude of the model errors into context (ideally model errors should be similar to or smaller than the uncertainty). Similar results have been found using other datasets and considering 2 subregions of SA: for TN, TX and precipitation over LPB (Carril et al. 2012), and for temperature extremes in southeast SA (Carril et al. 2016, this Special).

Fig. 3 shows the geographical distribution of seasonal mean TN and TX for DJF (first 2 columns) and JJA (last 2 columns), for the reference observational climatology (CRU, first row) and the model ensemble (RCM-ENS, second row). During DJF, the CRU climatology displays the highest temperatures (TN and TX) over the Gran Chaco region. During JJA, the highest TN values are located over the Amazon region, whereas the warmest region for TX is located more to the south at around 10°S. The LPB domain is characterized by a temperature gradient, mostly north–south oriented, which is especially evident for TX in JJA. In summer, as high values of TX occur inland over the northern and western part of this domain, the gradient has a zonal component, suggesting the influence of ocean as a temperature moderator. In general the main features of the distribution of TN and TX are well captured by the model ensemble during both seasons. The TN bias tends to be mostly positive throughout SA (i.e. models are warmer than the reference climatology), reaching maximum deviation with regard to the CRU climatology over Amazonia and central-northern Argentina. The TX bias is positive in the LPB and negative over Brazil. In both cases (TN and TX) the highest biases, in absolute value, are in the range of 2° to 4°C. The largest differences occur along the Andes, especially for TX which is underestimated. However, this bias should be interpreted with care, since the quality of observational datasets over areas with complex topography is critical for evaluating model performance (Solman et al. 2013). Similar spatial patterns of biases have been previously reported by Solman et al. (2013) and Sánchez et al. (2015) for seasonal mean surface air temperature, and by Carril et al. (2012) for TX in DJF and TN in JJA. The simulated TN and TX warming is largest between 10° and 35°S, affecting the LPB particularly in JJA (Fig. 3, third row). The projected changes in tropical regions are lower. In general, the changes in TN exhibit a greater level of confidence than those projected in TX. Geographic patterns of changes in TN and TX are similar to each other for each season. The warming in the LPB is larger in JJA than in DJF, implying that the amplitude of the seasonal cycle of temperature is projected to decrease.

3.2. Extreme temperature indices

Making an accurate estimate of the uncertainty in climate observations is a difficult task. To provide a useful measure of the uncertainty of extremes, we compare several alternative datasets (Covey et al. 2002) to put into context the magnitude of the errors of the simulations. Fig. 4 provides an overview of the differences in extreme indices, i.e. warm nights (TN90p), warm days (TX90p), cold nights (TN10p) and cold days (TX10p) (see Table 1 for definitions), estimated from different datasets (HadEX2, NCEP1, JRA-55 and RCM-ENS) for the period 1991–2010. The box-and-whisker plots display some basic statistics of the area-averaged extremes over NSA and SSA. The interquartile range (IQR, which is spanned by the 25th and 75th quantiles) provides an estimation of the variability of the extremes indices in each

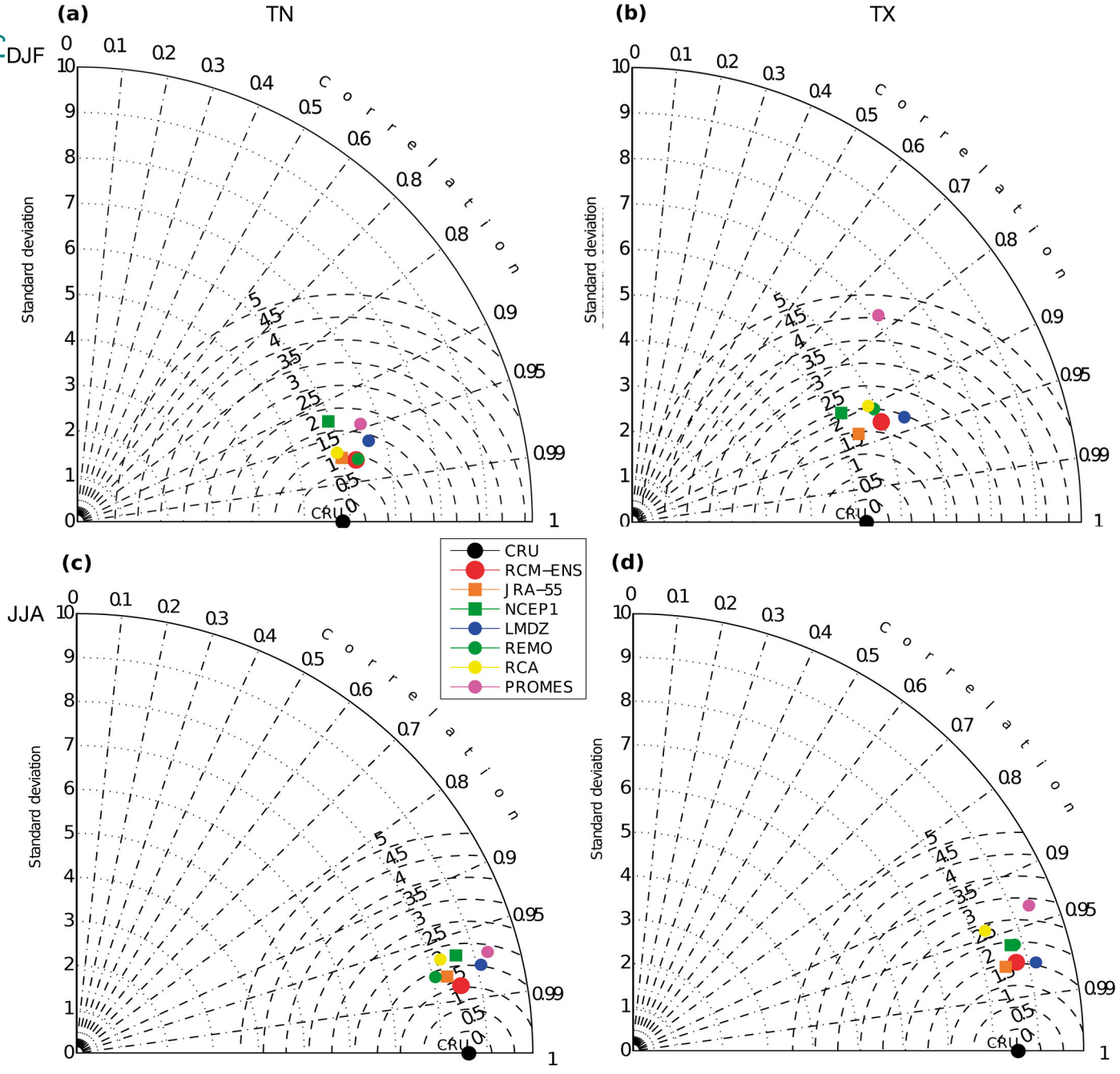

Fig. 2. Statistics displaying the spread of modeled and reanalysis summer (DJF) and winter (JJA) temperature indices (°C) for South America in the period 1991–2010 compared to the reference observational climatology (CRU, black point). Panels are Taylor diagrams (see Section 2: 'Data and methods'). Colored dots show values for individual regional models (PROMES, RCA, LMDZ and REMO), the ensemble mean (RCM-ENS) and NCEP1 and JRA-55 reanalyses. (a) Minimum temperature (TN), DJF; (b) maximum temperature (TX), DJF; (c) TN, JJA; (d) TX, JJA. Each panel illustrates three statistics: the standard deviation (vertical axis), the correlation coefficient (axial) and the mean root square error (concentric dashed lines around the CRU dot)

dataset. As in Carril et al. (2012), we consider the RCM-ENS as 'satisfactory' if its IQR intersects at least part of the corresponding IQR of HadEX2 and/or reanalysis data (a more strict criteria than just comparing the min.–max. ranges). In general, the criteria is fulfilled and the RCM-ENS match between the spread across the IQR of the other climatologies. Exceptions occur in SSA for indices based on TX (i.e. daytime extremes TX90p and TX10p; Fig. 4d,h). Moreover, the variability is larger for warm extremes (TN90p and TX90p; Fig. 4a–d) than for cold extremes (TN10p and TX10p; Fig. 4e–h). Variability peaks

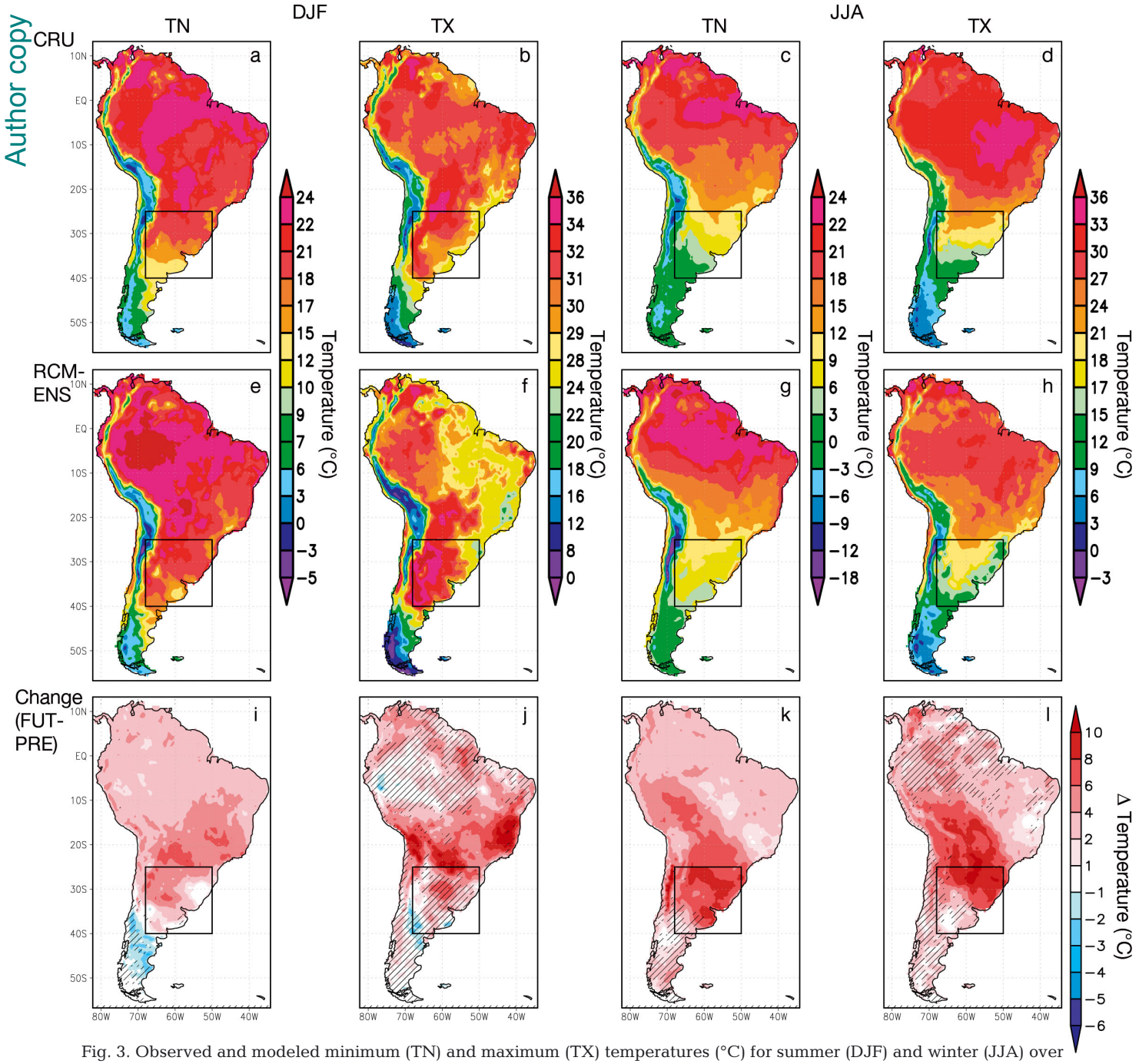

Fig. 3. Observed and modeled minimum (TN) and maximum (TX) temperatures (°C) for summer (DJF) and winter (JJA) over South America. Columns (left to right) show TN–DJF, TX–DJF, TN–JJA and TX–JJA. Rows (top to bottom) show observed values for the near-present (PRE) period (1991–2010) from the CRU dataset, the regional multi-model ensemble (MME) mean (RCM-ENS) for the same period, and changes projected (FUT) by RCM-ENS (2079–2098 minus 1991–2010). Hatching (bottom panels): anthropogenic climate change signal not significant at the 95% level

in NSA, where both IQR but also total min.–max. ranges display maximum values, and the RCM-ENS captures those characteristics. There is consensus among the datasets about the high frequency of occurrence of warm extremes (Fig. 4a–d). This is particularly notable in NSA, where mean values (Fig. 4a,c, left column) are clearly >10% (the mean expected value of the indices by definition, REF). However, the inter-dataset differences for warm extremes are also notable. For TX90p in NSA, the NCEP1 mean value lies outside the HadEX2 IQR (Fig. 4c, left panel), while for both TN90p and TX90p

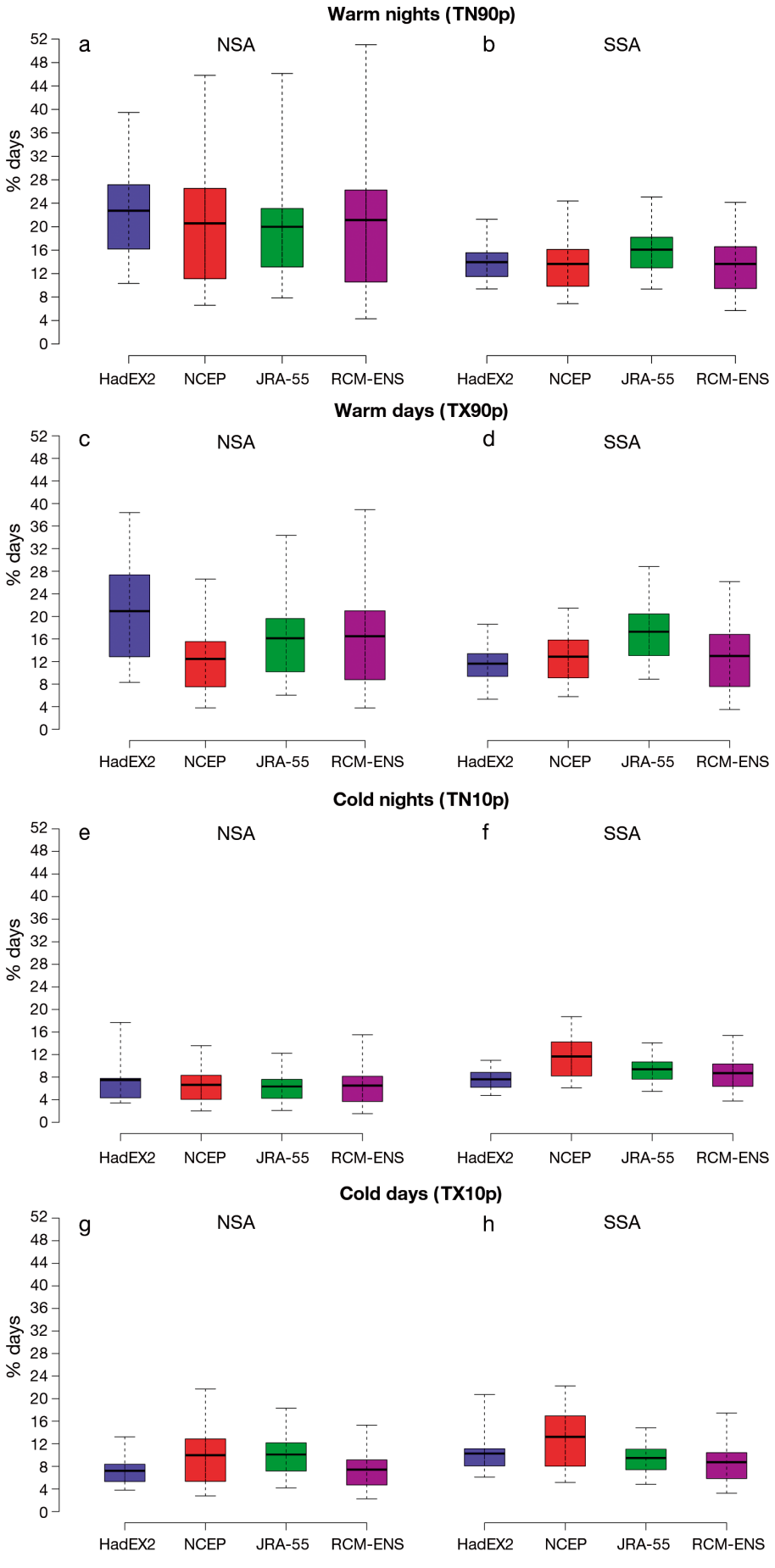

Fig. 4. Box-and-whisker plots of extreme temperature indices for northern South America (NSA, left panels) and southern South America (SSA, right panels) in 1991–2010, calculated from observational data (HadEX2 [blue]), reanalyses (NCEP1[red] and JRA-55 [green]) and the regional multi-model ensemble (RCM-ENS [purple]). (a,b) Warm nights (TN90p); (c,d) warm days (TX90p); (e,f) cold nights (TN10p); (g,h) cold days (TX10p). Boxes: interquartile range (IGR, i.e. the range between the 25th and 75th percentiles); black solid lines within the boxes: median; whiskers: maximum and minimum values. For the regional averages (NSA and SSA), a spatial-temporal variable mask according to the availability of the HadEX2 indices was applied

in SSA, JRA-55 is a warm biased dataset (Fig. 4b,d right column). On the other hand, there is consensus about the low frequency of occurrence of cold nights (TN10p) and days (TX10p) in NSA (Fig. 4e,g, left column), while in SSA (Fig. 4f,h right column) results are obscured by NCEP1 that appears as a cold biased dataset (with mean values outside the IQR of other climatologies).

The visual inspection of the spatial patterns of extremes from different datasets (Fig. 5) highlights the important degree of uncertainty obtained: the spread among indices of extremes from HadEx2, NCEP1 and JRA-55 is large. If we are to trust in the models' ability to simulate the near-present climate conditions, RCM-ENS errors (i.e. RCM-ENS minus HadEX2) need to be smaller than the uncertainty. Following Menéndez al. (2010a), uncertainty is defined here as the interclimatology range (i.e. HadEX2, NCEP1, JRA-55) of extreme indices (differences between the highest and the lowest value at each grid point). In this case, uncertainty is as large as the model errors over vast areas of SA, and the ensemble bias exceeds the uncertainty only in hatched regions (Fig. 5, bottom panels). It is worth noticing that RCMs used in this study were driven by atmospheric fields and sea surface temperatures from 'non-perfect' global coupled climate models (see Giorgi et al. 2009), in which chronology and some relevant processes (as e.g. land use changes) are missing. Only in case of RCMs driven by 'perfect boundary conditions' (i.e. from any reanalysis dataset) could we, ideally, expect models to agree with observations.

Projected changes in extreme indices are displayed in Fig. 6. RCM-ENS projects a significant warming over the whole continent by the end of the 21st century: the warm extremes are generally increased, while the cold extremes are diminished. In particular, the projected warming in nighttime extremes (TN) is larger than that in daytime extremes (TX).

In terms of change measured in percentage, the frequency of extreme warm nights (Fig. 6a) is projected to increase by up to the 80% in tropical SA, by about 50 to 70% in subtropical SA and by about 15 to 30% in SSA. A similar pattern of change is expected in extreme warm days (Fig. 6b), but to a lesser extent: in the majority of cases, their frequency in tropical and subtropical SA increases by <50%, while the southern portion of LPB is the region with the lowest sensitivity to climate change (<10%). In Amazonia, the larger increases in TN90p (Fig. 6a) compared with those of TX90p (Fig. 6b) are associated with projected increases in TN and not significant changes in TX (Fig. 3, bottom panels). In SSA different relationships are found for DJF and JJA. The small changes projected in the occurrence of warm nights (Fig. 6a) and days (Fig. 6b) in the LPB correspond well with small increases, or even decreases, in TN and TX in DJF (Fig. 3i,j).

On the other hand, projected changes in the number of cold nights/days are small (Fig. 6c,d). The largest changes are expected in the number of cold nights, and especially over the LPB and the Brazilian Highlands. These results of the projections are in agreement with the trends observed during the last decades of the 20th century (Rusticucci 2012, Skansi et al. 2013).

3.3. Factors influencing daily temperature extremes over the La Plata Basin

3.3.1. Cloud and surface radiative forcing

The relation of cloud and surface radiative forcing with TN and TX, under near present and future climate conditions is depicted in Fig. 7, which Rn, SWR, LWR, TN and TX as a function of TCC for DJF and JJA over the LPB domain. Here, 2 main factors are involved. The first is the role of cloudiness in decreasing TX during the daytime by reflecting solar radiation (i.e. reducing SWR). The second is greenhouse warming at night, which increases TN due to the infrared energy emitted by clouds returning to the surface (i.e. increasing LWR). Both processes tend to dampen the DTR for larger values of cloudiness (Zhou et al. 2009). Overall, RCM-ENS is able to capture these processes for both seasons: Fig. 7 shows that, as TCC decreases, SWR dominates and TX increases with Rn, while TN has an opposite and smaller slope. Increasing DTR with decreasing cloudiness is related to the corresponding increase of Rn. Furthermore, under future conditions (dashed lines) a generally larger increase of TN compared to TX is projected, especially in summer, associated

Fig. 5. Frequency of occurrence of temperature extremes (percentage of days in a year) in the near present period (1991–2010). Columns (left to right) show warm nights (TN90p), warm days (TX90p), cold nights (TN10p) and cold days (TX10p) (see Table 1 definitions of indices). Rows (top to bottom) show values from the HadEX2 observational dataset (areas with no data availability are masked), NCEP1 reanalysis, JRA-55 reanalysis, and the regional multi-model ensemble RCM-ENS. Hatching (bottom row): ensemble bias exceeds the uncertainty

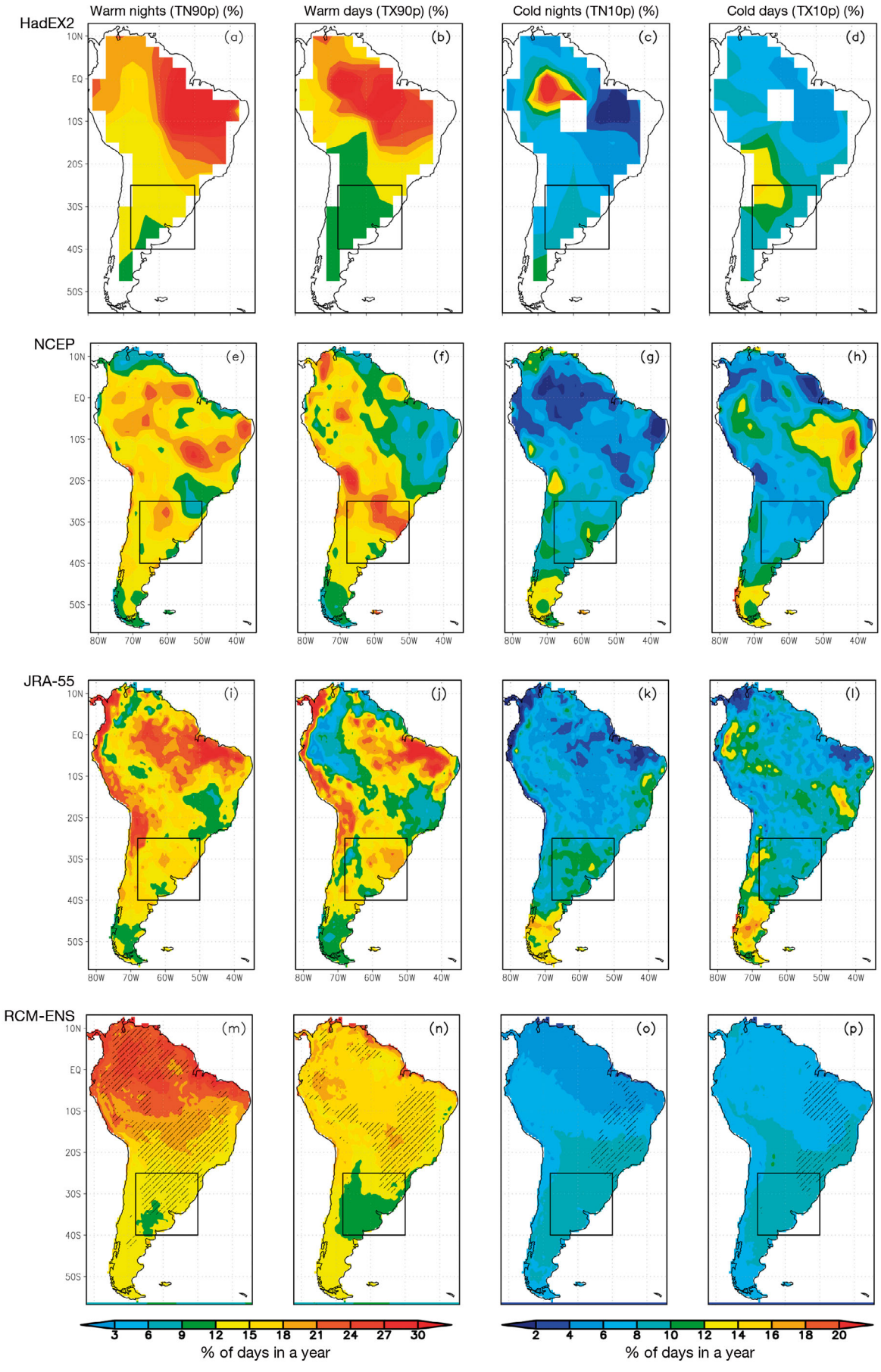
Warm nights (TN90p) (%)
Warm days (TX90p) (%)
Cold nights (TN10p) (%)
Cold days (TX10p) (%)
HadEX2
NCEP
JRA-55
RCM-ENS
(a)
(b)
(c)
(d)
(e)
(f)
(g)
(h)
(i)
(j)
(k)
(l)
(m)
(n)
(o)
(p)
10N
EQ
10S
20S
30S
40S
50S
80W
70W
60W
50W
40W
3 6 9 12 15 18 21 24 27 30
% of days in a year
2 4 6 8 10 12 14 16 18 20
% of days in a year

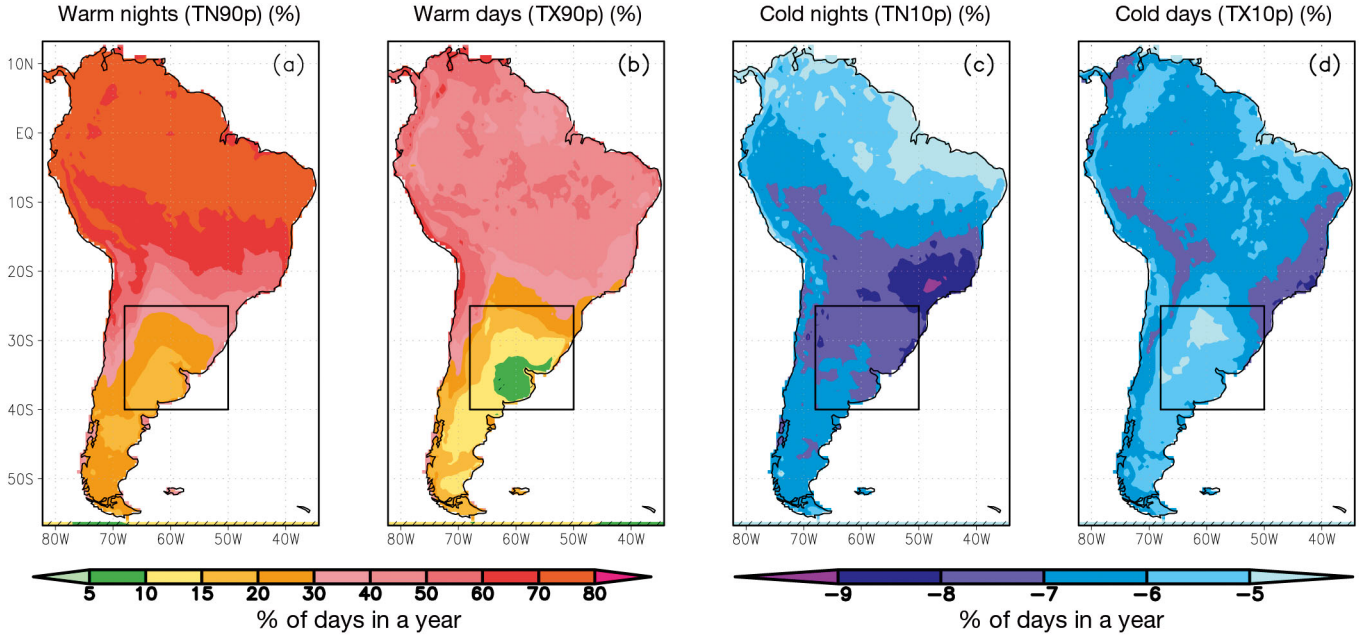

Fig. 6. Projected changes (2079–2098 minus 1991–2010) in the frequency of occurrence (percentage of days in a year) of temperature extremes over South Amercia. Values are means from the regional multi-model ensemble RCM-ENS. (a) Warm nights (TN10p), (b) warm days (TX90p), (c) cold nights (TN10p) and (d) cold days (TX90p). All changes are significant at the 95% level

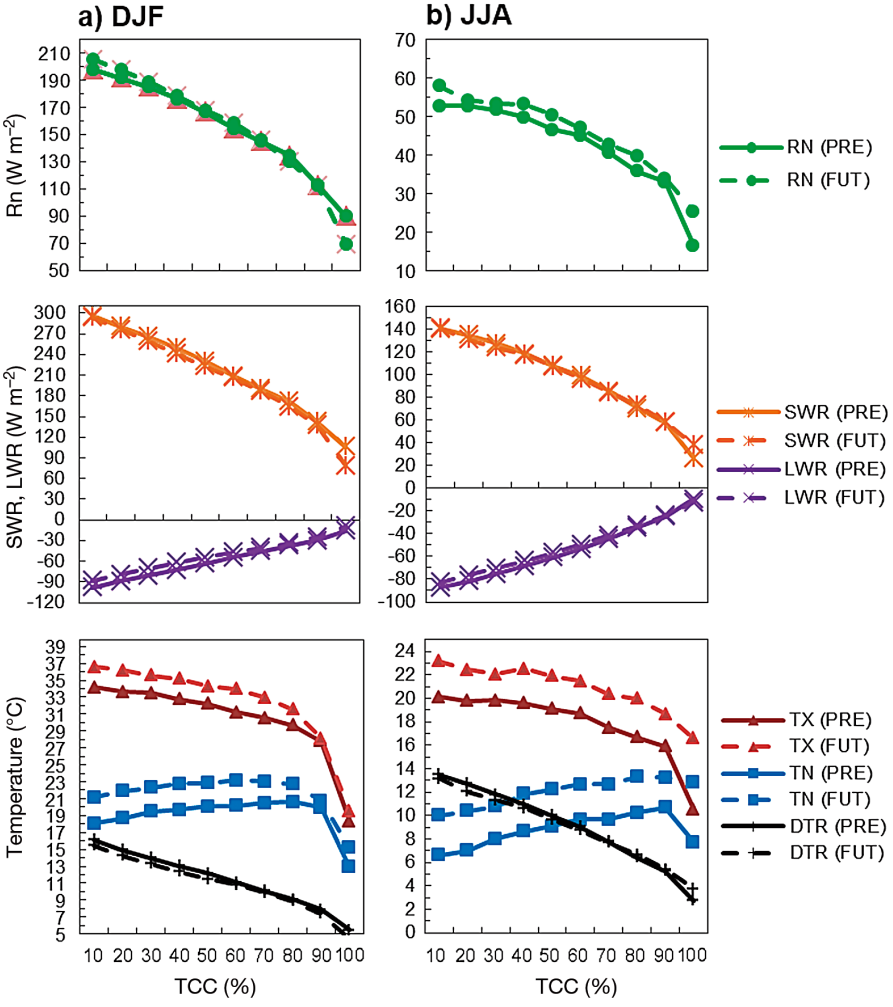

Fig. 7. Mean relation between total cloud cover (TCC) and other climate variables in summer (DJF, left panels) and winter (JJA, right panels) calculated by the regional multi-model ensemble RCM-ENS for the La Plata Basin (LPB). Rows (top to bottom) show TCC vs. surface net radiation (Rn); TCC vs. surface net downward shortwave flux (SWR) and surface net downward longwave flux (LWR); and TCC vs. minimum daily temperature (TN), maximum daily temperature (TX) and diurnal range temperature (DTR). PRE: near-present period (1991–2010, continuous lines); FUT: future period (2079–2098, dashed lines). Results are area averaged over the LPB domain. Note different *y*-axes for the 2 seasons

with increases of GHGs and decreases in the magnitude of LWR. Some differences are found between both extreme seasons. In the near-present period, the difference between warm and cold seasons is likely to be mainly related to SWR, as in winter the solar radiation is much weaker than in summer. In DJF (Fig. 7a, continuous lines), i.e. the austral summer, the magnitude of SWR (ranging from 100 to 300 Wm^{-2}), and consequently the temperatures, are higher than in JJA (Fig. 7b, continuous lines) (range 20 to 140 Wm^{-2}). Moreover, it is noticeable that RCM-ENS simulates a sharp reduction of TN in DJF and of TN and TX in JJA under TCC >90%, suggesting the possible influence of other processes related to frontal activity, precipitation and wetter soils. However, this nonlinear behavior between TCC and temperature is not reflected so clearly in DTR for high values of cloudiness.

Under SRES-A1B emissions scenario (Fig. 7, dashed lines), values under clear-sky conditions (left part of each panel) indicate the direct effect of increasing GHGs without the effect of clouds, while values under high cloudiness conditions (right part of each panel) show the combined effect of increasing GHGs and TCC. During DJF (Fig. 7a, dashed lines) RCM-ENS projects larger increases of TN than TX with in general somewhat larger changes of LW than of SW in conditions up to 70% TCC. This result is associated with larger increases of warm night temperatures (associated with TN) than of warm days (TX), as presented in Sections 3.1 and 3.2. The effect of GHGs is to keep the energy captured at the surface during the day, warming the surface at night. However, a strong nonlinear behavior regarding the relationship between TCC and both TN and TX is evident for TCC values >90%, with large decreases, relative to less cloudy conditions, in both temperatures. During the cold season (Fig. 7b, dashed lines), temperature and surface radiative forcing present qualitatively similar behavior as in DJF for TCC values up to 90%. However, for full cloud cover conditions, TX does not show a large decrease over less cloudy conditions, but shows a large increase over near-present climate conditions, both being qualitatively changes in opposition to what was observed in the DJF case. Fig. 8 shows the changes (expressed as absolute differences) in SWR, LWR and Rn as a function of TCC. LWR is projected to decrease in magnitude for both seasons, but especially in summer and for low cloudiness values (note that LWR has negative values). A marked decline of Rn in the case of total cloud cover conditions in DJF can be observed. Overall changes in SWR, LWR and Rn present a different pattern in DJF and JJA for TCC >90%. These results are in agreement with Zhou et al. (2009), who found that large decreases in DTR reflect the effects of TCC increases over the LPB domain under future conditions (see their Fig. 3). The lower projected increase in the occurrence of extremes in TX than TN over the LPB (Fig. 6) is also consistent with the decrease in DTR.

3.3.2. Meridional wind component influence

The dependence of TN and TX anomalies over the LPB upon the meridional wind component is shown in Fig. 9. For near present climate conditions and for both seasons, there is a high concordance between the sign of the meridional wind component and the sign of the temperature anomaly: northerly fluxes are

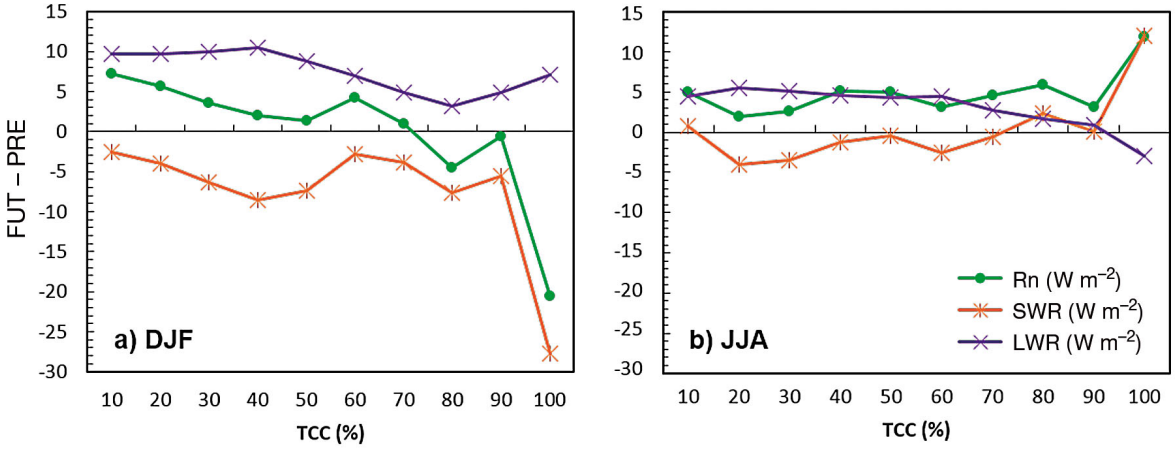

Fig. 8. Projected changes (2079–2098 minus 1991–2010) in the relation between total cloud cover (TCC) and surface net radiation (Rn), surface net downward shortwave flux (SWR) and surface net downward longwave flux (LWR) in (a) summer (DJF) and (b) winter (JJA) in the La Plata Basin. Results are area averaged over the LPB domain

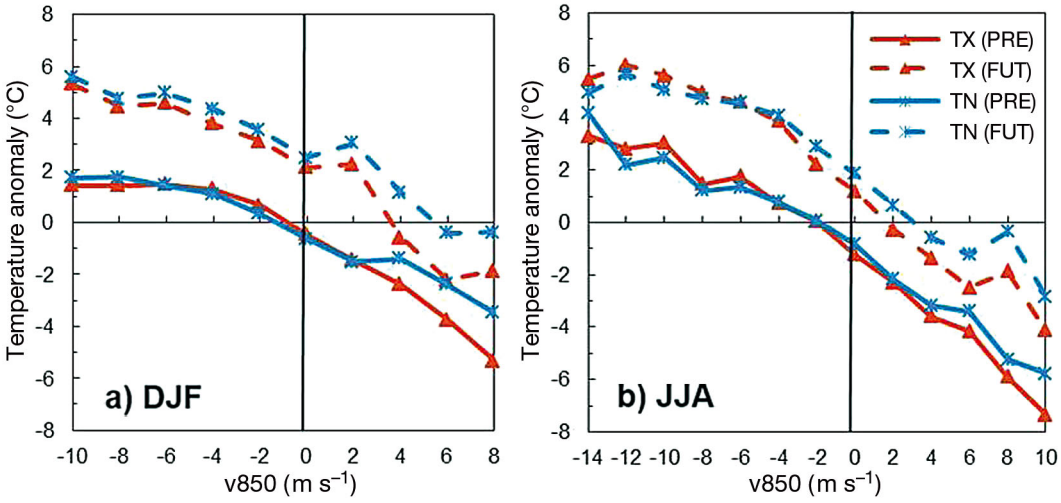

Fig. 9. Minimum temperature (TN) and maximum temperature (TX) anomalies (°C) related to meridional wind component at 850hP (v850, m s^{-1}) at 2 m s^{-1}intervals in (a) summer (DJF) and (b) winter (JJA) in the La Plata Basin (LPB). Results are area averaged over the LPB domain. Positive (negative) meridional wind values correspond with southerly (northerly) wind components. PRE: present period (1991–2010, continuous lines); FUT: future period (2079–2098, dashed lines)

associated with warm anomalies, while southerly fluxes are associated with cold anomalies. Under future climate conditions, the warming is evident in both seasons and for both TN and TX. Nevertheless, summertime cold anomalies only occur during those days in which the southerly wind component is greater than a certain threshold (Fig. 9a), i.e. 6 m s^{-1} (4 m s^{-1}) for anomalies in TN (TX). In winter (Fig. 9b), it is sufficient to have days with southerly wind component >2 m s^{-1} to have cold anomalies in both TN and TX.

Under present climate conditions (Fig. 9, continuous lines), the higher the northerly (southerly) wind component, the greater the positive (negative) temperature anomaly. However, the temperature is more sensitive to the southerly wind intensity (positive wind values in Fig. 9) than to the northerly wind intensity. Conversely, temperature is less sensitive to the intensity of the strongest northerly winds in DJF (Fig. 9a): northerly winds between –4 m s^{-1} and –10 m s^{-1} are associated with temperature anomalies of 1° to 2°C, while for southerly winds of 8 m s^{-1}, TN and TX anomalies are about –3°C and –5°C respectively. In winter (Fig. 9b) the temperature is more sensitive to intensity of the meridional wind component than in summer, and southerly wind component is associated with larger cold anomalies in TX than in TN.

In both periods, warm anomalies in TN are larger than those in TX in DJF (in JJA the relationship is less clear), while cold anomalies in TX are always larger than those in TN. Anomalies in TN and TX differ from each other much more clearly when the southerly wind component is large. In general, the difference between TN and TX anomalies are projected to increase in the future climate, especially for intense southerly winds.

4. SUMMARY AND CONCLUSIONS

This study analyzes the seasonal mean fields of maximum and minimum daily temperature and 4 ETCCDI indices of extreme temperatures under near-present (1990–2010) and future climate conditions (2079–2098). Several observational databases and reanalyses are used to evaluate the uncertainty linked to the use of regional models and to put into context the biases of a set of 4 RCMs when reproducing the regional mean climate and extreme features. The influence of the cloudiness, the radiative forcing and the meridional winds on temperature anomalies are also analyzed, focusing on the LPB region.

The RCM-ENS captures the regional spatial features of the seasonal mean TN and TX better than any of the individual models. However, warm biases are identified over the Amazon basin and LPB, and cold biases are found in orographic areas with high altitude and in Patagonia especially during the austral summer.

Despite this uncertainty in the data, the simulation of warm/cold days/nights by the RCM-ENS is satisfactory, fulfilling the criterion of matching between the spread across the interquartile range of the other climatologies (HadEX2, NCEP1 and JRA-55). In particular, there is consensus among the climatologies that variability of warm extremes (TN90p, TX90p)

is larger than variability of cold extremes (TN10p, TX10p), with maximum variability in NSA. According to results from RCM-ENS and HadEX2, during the near present period, LPB is a region with relatively low frequency of occurrence of warm extremes (TN90p and TX90p). These results are in agreement with previous findings based on observational data (Rusticucci 2012, Skansi et al. 2013).

At the end of 21st century, RCM-ENS depicts a consistent picture between the projected changes of seasonal mean TX and TN and changes in temperature extremes. Areas where the warm nights increase more than warm days are also those where TN increases more than TX in summer, as it is the case for the LPB where the lowest warming of TX is projected. A contributory factor limiting the increase in TX is the response of summer precipitation and evapotranspiration in the LPB (Menéndez et al. 2016).

The reflective cooling and greenhouse effects of TCC on TX, TN and DTR are analyzed. The influence of clouds has opposite effects on night- and daytime processes. While their property of absorbing outgoing radiation affects principally TN, their property of reflecting solar radiation has a direct influence on TX. In the LPB, the RCM-ENS projects larger changes for LWR than for SWR. RCM-ENS simulates a nearly linear relationship between temperature and cloudiness for TCC values up to 90% (decreased TX and increased TN as TCC increases). However, for very cloudy to full cloud cover conditions, this slope is usually sharply reversed, suggesting a cooling effect connected to other processes such as rainfall and frontal passages. The different behavior for high values of TCC is also reflected in Rn. Changes in TN and TX simulated by RCM-ENS are consistent with a reduction in DTR on LPB. The same conclusion can be drawn from data presented by Zhou et al. (2009, their Fig. 2), in which the LPB is identified as the area of SA where the largest decrease in DTR is projected. We find here that this decrease occurs in summer and winter and for any value of TCC (except for high cloudiness in JJA), and is larger on days with low cloudiness.

We also examine how the intensity of the meridional wind component influences TN and TX anomalies under near present and future climate conditions. During the 2079–2098 future period and for summer conditions, warm anomalies (relative to the near present climate) are exhibited on all days except for those with a strong southerly flow (which represent <1% of the days; data not shown). In general, temperature is more sensitive to the intensity of the meridional flow in winter than in summer, and it is more sensitive to southerly winds than northerly winds. Moreover, southerly winds are associated with larger negative anomalies in TX than in TN. The separation between the TN and TX anomalies is larger by the end of the 21st century than during the near-present climate, no matter what the wind speed is, although this is more evident when the wind is from the south.

The study demonstrates that RCMs are a valuable tool for the study of daily temperature extremes at regional scales. Crucially, they can be used over regions where the observational datasets are scarce, as it is the case of SA. Furthermore, RCMs can simulate in a physically-consistent way the influence of cloud cover, radiative fluxes and meridional wind over the daily temperature extremes, despite the inherent limitations involved in modelling the complex interrelationship between these variables. The results obtained will serve as the basis for further studies that should take into account other features and climatic mechanisms such as soil moisture, evapotranspiration, rainfall, and humidity advection. It is clearly necessary to perform further analysis of other related physical processes that could affect the behavior and characteristics of daily temperatures extremes over the LPB and other regions of SA.

Acknowledgements. This work was supported by the European Community's Seventh Framework Programme (CLARIS-LPB, Grant Agreement No 212492), by the Argentinean agencies CONICET (PIP 11220110100932, PIP 11220150100402CO) and ANPCyT (PICT-2014-0887) and by the French National Programme LEFE/INSU (AO 2015-876370).

LITERATURE CITED

Aguilar E, Aziz Barry A, Brunet M, Ekang L and others (2009) Changes in temperature and precipitation extremes in western central Africa, Guinea Conakry, and Zimbabwe, 1955–2006. J Geophys Res 114:D02115, doi: 10.1029/2008JD011010

Alexander LV, Zhang X, Peterson TC, Caesar J and others (2006) Global observed changes in daily climate extremes of temperature and precipitation. J Geophys Res Atmos 111:1–22

Andrade C, Leite SM, Santos JA (2012) Temperature extremes in Europe: overview of their driving atmospheric patterns. Nat Hazards Earth Syst Sci 12:1671–1691

Bambrick HJ, Capon AG, Barnett GB, Beaty RM, Burton AJ (2011) Climate change and health in the urban environment: adaptation opportunities in Australian cities. Asia Pac J Public Health 23 Suppl:67S–79S

Beniston M, Stephenson DB (2004) Extreme climatic events and their evolution under changing climatic conditions. Global Planet Change 44:1–9

Betts AK, Desjardins R, Worth D (2013) Cloud radiative forcing of the diurnal cycle climate of the Canadian Prairies.

J Geophys Res Atmos 118:8935–8953

Carril AF, Menéndez CG, Remedio ARC, Robledo F and others (2012) Performance of a multi-RCM ensemble for South Eastern South America. Clim Dyn 39:2747–2768

Carril AF, Cavalcanti IFA, Menéndez CG, Sörensson A and others (2016) Extreme events in the La Plata Basin: a retrospective analysis of what we have learned during the CLARIS-LPB project. Clim Res 68:95–116

Castro M, Fernandez C, Gaertner MA (1993) Description of a meso-scale atmospheric numerical model. In: Diaz JI, Lions JL (eds) Mathematics, climate and environment. Masson, Paris, p 230–235

Covey C, Achuta Rao KM, Fiorino M, Gleckler PJ, Taylor KE, Wehner MF (2002) Intercomparison of climate data sets as a measure of observational uncertainty. Report no. 69, Program for Climate Model Diagnosis and Intercomparison, Lawrence Livermore National Laboratory, Livermore, CA

Dai A, Trenberth KE, Karl TR (1999) Effects of clouds, soil moisture, precipitation, and water vapor on diurnal temperature range. J Clim 12:2451–2473

Donat MG, Alexander LV, Yang H, Durre I and others (2013) Updated analyses of temperature and precipitation extreme indices since the beginning of the twentieth century: the HadEX2 dataset. J Geophys Res Atmos 118: 2098–2118

Flato G, Marotzke J, Abiodun B, Braconnot P others (2013) Evaluation of Climate Models. In: Stocker TF et al. (eds) Climate change 2013: the physical science basis. Contribution of Working Group I to the fifth assessment report of the Intergovernmental Panel on Climate Change. Cambridge University Press, Cambridge, p 741–866

Frich P, Alexander LV, Della-Marta P, Gleason B, Haylock M, Tank Klein MG, Peterson T (2002) Observed coherent changes in climatic extremes during the second half of the twentieth century. Clim Res 19:193–212

Garreaud R (2000) Cold air incursions over subtropical South America: mean structure and dynamics. Mon Weather Rev 128:2544–2559

Garreaud RD, Vuille M, Compagnucci R, Marengo J (2009) Present-day South American climate. Palaeogeogr Palaeoclimatol Palaeoecol 281:180–195

Giorgi F, Francisco R (2000) Uncertainties in regional climate change prediction: a regional analysis of ensemble simulations with the HADCM2 coupled AOGCM. Clim Dyn 16:169–182

Giorgi F, Jones C, Asrar G (2009) Addressing climate information needs at the regional level: the CORDEX framework. WMO Bull. 58:175–183

Gordon C, Cooper C, Senior CA, Banks H and others (2000) The simulation of SST, sea ice extents and ocean heat transports in a version of the Hadley Centre coupled model without flux adjustments. Clim Dyn 16: 147–168

Harris I, Jones PD, Osborn TJ, Lister DH (2014) Updated high-resolution grids of monthly climatic observations—the CRU TS3.10 Dataset. Int J Climatol 34:623–642

Hartmann DL, A.M.G. Klein Tank AMG, M. Rusticucci M, L.V. Alexander LV and others (2013) Observations: atmosphere and surface. In: Stocker TF et al. (eds) Climate change 2013: the physical science basis. Contribution of Working Group I to the fifth assessment report of the Intergovernmental Panel on Climate Change. Cambridge University Press, Cambridge, p 159–254

Hourdin F, Musat I, Bony S, Braconnot P and others (2006) The LMDZ4 general circulation model: climate performance and sensitivity to parametrized physics with emphasis on tropical convection. Clim Dyn 27:787–813

Jacob D, Elizalde A, Haensler A, Hagemann S and others (2012) Assessing the transferability of the regional climate model REMO to different COordinated Regional climate Downscaling EXperiment (CORDEX) regions. Atmosphere 3:181–199

Kalnay E, Kanamitsu M, Kistler R, Collins W and others (1996) The NCEP/NCAR 40-year reanalysis project. Bull Am Meteorol Soc 77:437–471

Kendon EJ, Rowell DP, Jones RG, Buonomo E (2008) Robustness of future changes in local precipitation extremes. J Clim 21:4280–4297

Kobayashi S, Ota Y, Harada Y, Ebita A and others (2015) The JRA-55 reanalysis: general specifications and basic characteristics. J Meteorol Soc Japan 93:5–48

Kodra E, Ganguly AR (2014) Asymmetry of projected increases in extreme temperature distributions. Sci Rep 4:5884, doi:10.1038/srep05884

Lavell A, Oppenheimer M, Diop C, Hess J and others (2012) Climate change: new dimensions in disaster risk, exposure, vulnerability, and resilience. In: Field CB, Barros V, Stocker TF, Qin D and others (eds) Managing the risks of extreme events and disasters to advance climate change adaptation. Special report of Working Groups I and II of the Intergovernmental Panel on Climate Change. Cambridge University Press, Cambridge, p 25–64

Li L (1999) Ensemble atmospheric GCM simulation of climate interannual variability from 1979 to 1994. J Clim 12: 986–1001

Lindvall J, Svensson G (2014) The diurnal temperature range in the CMIP5 models. Clim Dyn 44:405–421

Marengo JA, Jones R, Alves LM, Valverde MC (2009) Future change of temperature and precipitation extremes in South America as derived from the precis regional climate modeling system. Int J Clim 29:2241–2255

Menéndez CG, de Castro M, Boulanger JP, D'Onofrio A and others (2010a) Downscaling extreme month-long anomalies in southern South America. Clim Change 98:379–403

Menéndez CG, de Castro M, Sörensson A, Boulanger JP (2010b) CLARIS project: towards climate downscaling in South America. Meteorol Zeitschrift 19:357–362

Menéndez CG, Zaninelli PG, Carril AF, Sánchez E (2016) Hydrological cycle, temperature and land surface–atmosphere interaction in the La Plata Basin during summer: response to climate change. Clim Res 68:231–241

Nakicenovic N, Swart R (eds) (2000) Emissions scenarios. Special report of Working Group III of the Intergovernmental Panel on Climate Change. Cambridge University Press, Cambridge

Plavcová E, Kyselý J (2011) Evaluation of daily temperatures in Central Europe and their links to large-scale circulation in an ensemble of regional climate models. Tellus, Ser A, Dyn Meterol Oceanogr 63:763–781

Plavcová E, Kyselý J (2012) Atmospheric circulation in regional climate models over Central Europe: links to surface air temperature and the influence of driving data. Clim Dyn 39:1681–1695

Rangwala I, Barsugli J, Cozzetto K, Neff J, Prairie J (2012) Mid-21st century projections in temperature extremes in the southern Colorado Rocky Mountains from regional climate models. Clim Dyn 39:1823–1840

Roeckner E, Brokopf R, Esch M, Giorgetta M, and others (2006) Sensitivity of simulated climate to horizontal and

vertical resolution in the ECHAM5 atmosphere model. J Clim 19:3771–3791

Ruscica RC, Menéndez CG, Sörensson AA (2016) Land surface–atmosphere interaction in future South American climate using a multi-model ensemble. Atmos Sci Lett 17:141–147

Rusticucci M (2012) Observed and simulated variability of extreme temperature events over South America. Atmos Res 106:1–17

Rusticucci M, Barrucand M (2004) Observed trends and changes in temperature extremes over Argentina. J Clim 17:4099–4107

Samuelsson P, Jones CG, Willén U, Ullerstig A and others (2011) The Rossby Centre regional climate model RCA3: model description and performance. Tellus A 63:4–23

Sánchez E, Solman S, Remedio ARC, Berbery H and others (2015) Regional climate modelling in CLARIS-LPB: a concerted approach towards twenty first century projections of regional temperature and precipitation over South America. Clim Dyn 45:2193–2212

Sillmann J, Kharin VV, Zhang X, Zwiers FW, Bronaugh D (2013a) Climate extremes indices in the CMIP5 multimodel ensemble: 1. Model evaluation in the present climate. J Geophys Res Atmos 118:1716–1733

Sillmann J, Kharin VV, Zwiers FW, Zhang X, Bronaugh D (2013b) Climate extremes indices in the CMIP5 multimodel ensemble: 2. Future climate projections. J Geophys Res Atmos 118:2473–2493

Sillmann J, Donat MG, Fyfe JC, Zwiers FW (2014) Observed and simulated temperature extremes during the recent warming hiatus. Environ Res Lett 9:064023, doi:10.1088/1748-9326/9/6/064023

Skansi MM, Brunet M, Sigró J, Aguilar E and others (2013) Warming and wetting signals emerging from analysis of changes in climate extreme indices over South America. Global Planet Change 100:295–307

Solman SA, Sanchez E, Samuelsson P, da Rocha RP and others (2013) Evaluation of an ensemble of regional climate model simulations over South America driven by the ERA-Interim reanalysis: model performance and uncertainties. Clim Dyn 41:1137–1157

Sörensson AA, Menéndez CG (2011) Summer soil-precipitation coupling in South America. Tellus A 63:56–68

Stephenson DB 2008: Definition, diagnosis and origin of extreme weather and climate events. In: Diaz HF, Murname RJ (eds) Climate Extremes and Society. Cambridge University Press, Cambridge, p 11–23

Stone A, Weaver J (2003) Factors contributing to diurnal temperature range trends in twentieth and twenty-first century simulations of the CCCma coupled model. Clim Dyn 20:435–445

Taylor KE (2001) Summarizing multiple aspects of model performance in a single diagram. J Geophys Res Atmos 106:7183–7192, doi:10.1029/2000JD900719

Tencer B, Rusticucci M, Jones P, Lister D (2011) A southeastern South American daily gridded dataset of observed surface minimum and maximum temperature for 1961–2000. Bull Am Meteorol Soc 92:1339–1346

Thibeault JM, Seth A (2014) Changing climate extremes in the Northeast United States: observations and projections from CMIP5. Clim Change 127:273–287

Vincent LA, Peterson TC, Barros VR, Marino MB and others (2005) Observed trends in indices of daily temperature extremes in South America 1960–2000. J Clim 18: 5011–5023

You Q, Kang S, Aguilar E, Pepin N and others (2011) Changes in daily climate extremes in China and their connection to the large scale atmospheric circulation during 1961–2003. Clim Dyn 36:2399–2417

Zaninelli P, Carril AF, Menéndez CG 2015: explorando temperaturas máximas y mínimas en diferentes reanálisis. 1. Campos medios estacionales. Meteorologica 40:43–58

Zhang X, Alexander L, Hegerl GC, Jones P and others (2011) Indices for monitoring changes in extremes based on daily temperature and precipitation data. Wiley Interdiscip Rev Clim Chang 2:851–870

Zhou L, Dickinson RE, Dirmeyer P, Dai A, Min SK (2009) Spatiotemporal patterns of changes in maximum and minimum temperatures in multi-model simulations. Geophys Res Lett 36: L02702, doi:10.1029/2008GL036141

Editorial responsibility: Christine Paetzold, Oldendorf/Luhe, Germany

Submitted: June 4, 2015; Accepted: January 5, 2016
Proofs received from author(s): April 25, 2016